Electrical connections and driving electronics for piezo-actuated x-ray thin glass optics

Ugo Lo Cicero, Luisa Sciortino, Giuseppe Lullo, Maurizio Di Bella, Marco Barbera, et al.

Ugo Lo Cicero, Luisa Sciortino, Giuseppe Lullo, Maurizio Di Bella, Marco Barbera, Alfonso Collura, Roberto Candia, Daniele Spiga, Stefano Basso, Marta Civitani, Carlo Pelliciari, Bianca Salmaso, "Electrical connections and driving electronics for piezo-actuated x-ray thin glass optics," Proc. SPIE 9965, Adaptive X-Ray Optics IV, 99650A (27 October 2016); doi: 10.1117/12.2237910

SPIE.

Event: SPIE Optical Engineering + Applications, 2016, San Diego, California, United States

Electrical connections and driving electronics for piezo-actuated x-ray thin glass optics

Ugo Lo Cicero*[a], Luisa Sciortino[b], Giuseppe Lullo[c], Maurizio Di Bella[a], Marco Barbera[b,a], Alfonso Collura[a], Roberto Candia[a], Daniele Spiga[d], Stefano Basso[d], Marta Civitani[d], Carlo Pelliciari[d], Bianca Salmaso[d]

[a] INAF - Osservatorio Astronomico di Palermo, Piazza del Parlamento 1, 90134 Palermo (Italy)
[b] Università degli Studi di Palermo, Dip. Di Fisica e Chimica, Via Archirafi 36, 90123 Palermo (Italy)
[c] Università degli Studi di Palermo, Dip. Di Energia, Ingegneria dell'Informazione e Modelli Matematici, Viale delle Scienze, Ed. 9, 90128 Palermo (Italy)
[d] INAF – Osservatorio Astronomico di Brera, Via Bianchi 46, 23807 Merate (Italy)

ABSTRACT

Use of thin glass modular optics is a technology currently under study to build light, low cost, large area X-ray telescopes for high energy astrophysics space missions. The angular resolution of such telescopes is limited by local deviations from the ideal shape of the mirrors. One possible strategy to improve it consists in actively correcting the mirror profile by gluing thin ceramic piezo-electric actuators on the back of the glasses. A large number of actuators, however, requires several electrical connections to drive them with the different needed voltages. We have developed a process for depositing conductive paths directly on the back of non-planar thin foil mirrors by means of a photolithographic process, combined with metal thin film evaporation and selective removal. We have also designed and built a modular multichannel electronic driver with each module capable of driving simultaneously up to 16 actuators with a very low power consumption. Here we present our electrical interconnections technology and the solutions adopted in the implementation of the electronics.

Keywords: Active X-ray optics, thin glass optics, piezoelectric actuators, piezoelectric multichannel drivers, interconnections patterning, X-ray telescope mirrors.

1 INTRODUCTION

1.1 X-ray telescopes

New X-ray astrophysics space observatories need large, high effective area, high angular resolution, lightweight, grazing-incidence optics at a reasonable cost. The acceptable compromise between the desired characteristics strongly depends on the peculiarity of each mission, and new technologies are on their way to improve all of these aspects. One of these technologies under development makes use of a thin glass foil as base reflecting element [1]. Thin slumped glass foils optics have been proposed as an alternative to silicon pore optics (the current baseline of the ATHENA mission) for next-generation X-ray telescopes [2], and have already been successfully employed for the NuSTAR (Nuclear Spectroscopic Telescope Array) mission [3].

* locicero@astropa.inaf.it; phone +39 091 233 621

Adaptive X-Ray Optics IV, edited by Stephen L. O'Dell, Ali M. Khounsary, Proc. of SPIE Vol. 9965, 99650A · © 2016 SPIE · CCC code: 0277-786X/16/$18 · doi: 10.1117/12.2237910

1.2 Thin glass optics

A thin glass optics assembly comprise a number of modules typically mounted in a Wolter-I configuration (two reflections in sequence onto a paraboloidal and hyperboloidal surface), each one being a stack of shaped thin glass foils. The curvature of the glasses can be obtained by a low-cost replication process. The hot slumping in use at INAF-OAB allows to curve the glasses along the longitudinal axis, endowing the foils with a cylindrical shape. A subsequent integration onto a precisely shaped parabolic/hyperbolic mold exploits the elasticity of the glass, to impart the final shape. For this purpose, an Integration MAchine (IMA) has been specifically developed and utilized at INAF-OAB. The final glass shape is then held by rigid glass ribs glued to the foil on one side, and to a stiff backplane on the other (or to the previously integrated foil in the stack), that also serve as spacers to stack several glasses together [4].

1.3 Shape correction

High glass quality makes possible to build optics with a smooth surface, but the shaping method still produces residual waviness and mid-frequency shape imperfections that affect the angular resolution of the optics (even though with improving performances [5]). A possibility to correct these defects consists in actively adjusting the shape of the optics through piezoelectric actuators. We tested this technology by gluing an array of tangentially-acting actuators on the back of prototype thin glass optics [6] [7] [8].

2 ELECTRICAL CONNECTIONS

2.1 Requirements

To test shape correction, we need to individually control each actuator with voltages in the range of ±100 V. In order to obtain scalable, robust, un-obstructive interconnections we deposited a pattern of electrical tracks directly on the back of the glass, with pads to which the piezo contacts can be electrically connected via a conductive glue. The actuators are mechanically anchored to the glass by a low shrinkage epoxy glue, only applied to the active area of the piezoelectric patches.

The electrical interconnections must be thin enough not to exert a mechanical stress capable of deforming the glass. Their thickness has to be small enough to avoid mechanical interference with the ribs, i.e., they shall not exceed the thickness of the glue that fixes the ribs to the glass. We verified that the glass shows negligible deformations induced by the tracks if their thickness does not exceed 95 nm and their width is less than 2 mm. As shown in metrology reported in Figure 1, the majority of the deformations stays in the range of ±0.1 μm both before and after the deposition, and the visible changes are not geometrically correlatable to the tracks path.

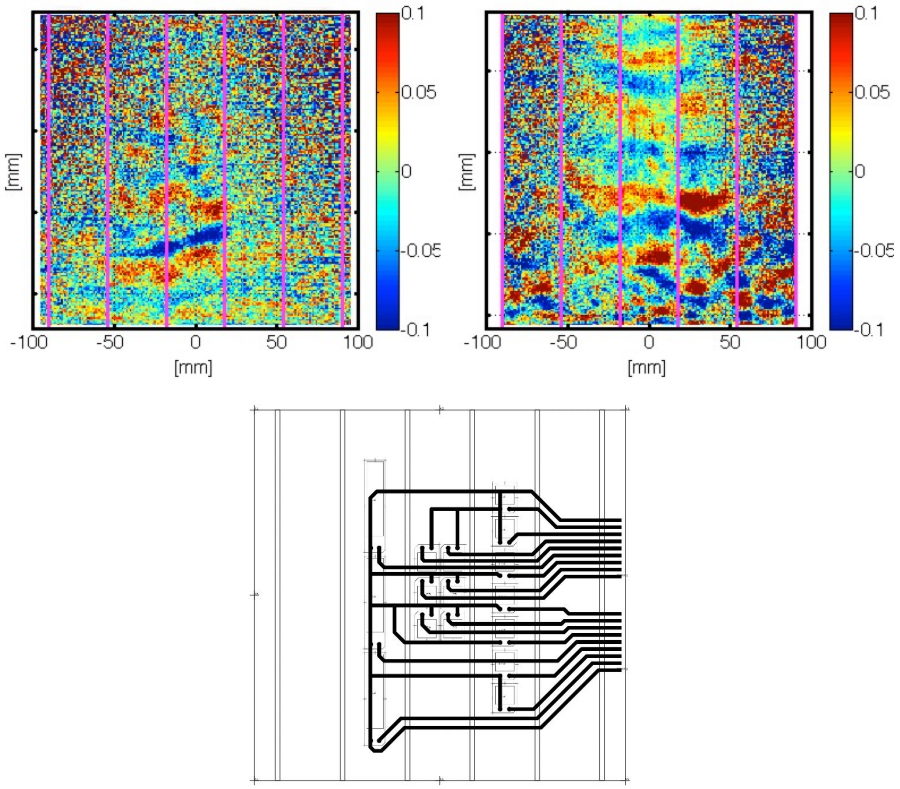

Figure 1. Residual maps with respect to a cylinder with 1 m radius of curvature, after removing the best-fit Legendre polynomials up to the eight order. Before (up-left) and after (up-right) electrical tracks deposition with pattern shown in the bottom image. Error range is not significantly changed. The colorbar is graded in microns.

The tracks adhesion on the glass has to be excellent to ensure robustness. We employed titanium as metal for the tracks since it shows a very good adhesion to the glass, covered with an additional layer of gold that protects the titanium against oxidation and is used as etching mask during the patterning process (Sect. 2.2). Electrical conductivity is not a main issue, since the impedance of the actuators is very high, over 1 GΩ, so even a line resistance of tens of kiloohms would produce a voltage drop of only few millivolts.

2.2 Deposition and patterning

The glass samples over which we deposited the electrical tracks were 0.4 mm thick, 20 cm x 20 cm Corning Eagle glass sheets, shaped by hot slumping to obtain a cylindrical curvature with 1 m curvature radius [9]. The patterning process was developed at INAF-OAPA micro-technologies laboratory.

The first step of the process consisted of depositing an 80 nm film of titanium and a 15 nm film of gold on the glass using a Varian high-vacuum e-beam evaporator.

A DuPont Riston MM540 dry film negative photoresist was then applied to the metalized glass by lamination, using a commercial plastic-lamination machine. The high elasticity of the glass allows the safe passage through the rollers of the laminator. The glass side not in contact with the photoresist was protected, during the lamination, by an optical paper cloth, to avoid damaging or contaminating the optical surface. The lamination consisted of three passages through the laminator set at 110 °C; higher temperatures would make the photoresist reflow, worsening its uniformity, while lower ones would not assure a good adherence of the photoresist on the glass. Dry photoresist solves the issue of low wettability of glass when using liquid photoresist; in fact, our process was previously based on spray application of

photoresist, with thermal treatment of the glass to assure uniformity. When switching from different kinds of glass to the Corning Eagle, it was noticed that its wettability to photoresist was especially low and non-uniform, yielding to inhomogeneous and uneven resist layer, which in turn produced damaged tracks.

The sample was then put in a MEGA AZ210 UV exposure unit. An inkjet printed mask, reproducing the inverted pattern of the tracks to be obtained, was placed on the photoresist-covered side and pressed by a thick slab of glass, once again exploiting the elasticity of the thin glass. Flattening the glass allowed us to obtain a uniform photoresist exposure. The photoresist was exposed for 25 s and developed in a Na_2CO_3 based solution for 2.5 min.

After rinsing in De-Ionized Water (DIW) the glass was dipped in aqua regia (HNO_3:HCl 1:3) for 20 s to etch the exposed gold through the opened photoresist window. Once rinsed again in DIW, the sample was dipped in H_2O_2 (30%) for 1 h to etch the titanium. The already patterned gold acts as mask to protect the titanium from the etching were the track have to be patterned, so the photoresist is not needed anymore, but it only provides an extra protection to the titanium; in fact, the photoresist adherence to the glass is highly reduced during this etching phase, and some parts can easily detach from the glass.

The sample was then rinsed in DIW and the residual photoresist was removed with acetone. The result is shown in Figure 2 and Figure 3: the piezoelectric actuators are glued to the glass during the integration process, as shown in Figure 4.

Figure 2. Electric tracks deposited on the back of a curved thin glass. They are still protected by a photoresist film.

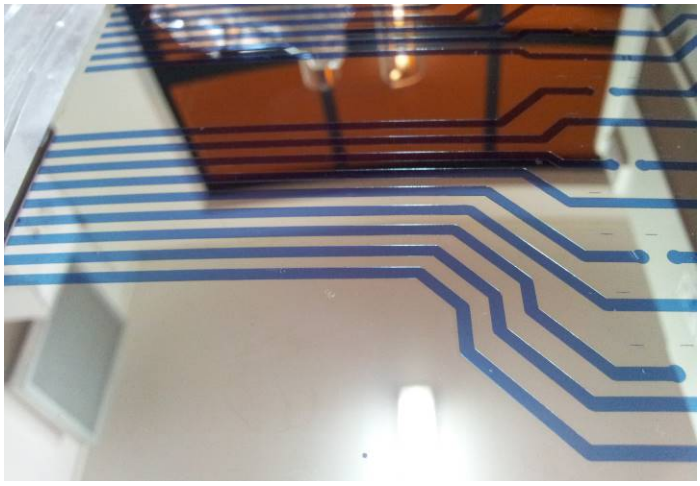

Figure 3. Detail of deposited tracks. Small size alignment features are visible on the right.

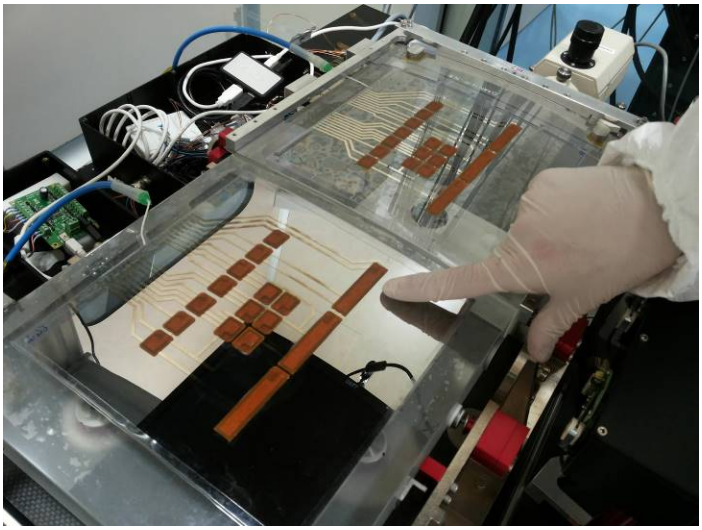

Figure 4. Piezoelectric actuators glued to glass foils during the integration process in the IMA.

2.3 Ad-hoc connector and flex cables

All the electrical tracks end in two groups of pads. In order to connect the external pads to the wirings we built an ad-hoc connector based on copper-beryllium springs soldered to a specifically shaped PCB (Printed Circuit Board), that provides a stable connection while exerting a low pressure to avoid damaging the pads or the glass Figure 5). Multiple insertions did not show any damage to the deposited metal pads.

We linked the connector to the driving electronics through a flex cable built by photolithography from a copper-plated polyimide strip (Figure 5). This cable is very flexible and minimizes the forces applied to the glass that could translate into deformations (Figure 6).

Figure 5. Ad-hoc connector and flex cable attached to the glass.

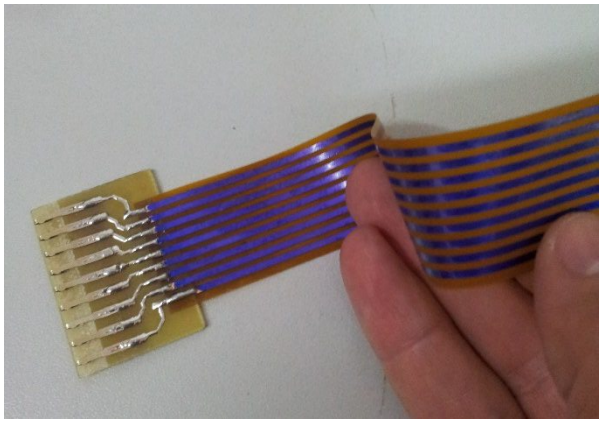

Figure 6. Flex cable soldered to ad-hoc connector. The high flexibility of the cable avoids mechanical stress to the glass.

3 PIEZO DRIVE ELECTRONICS

3.1 Requirements for preliminary testing

After a number of preliminary consideration and tests, the choice for piezo-electric actuators fell on two devices manufactured by Physik Instrumente: model P-876.SP1, having a size of 16 mm × 13 mm and a measured capacitance of around 6 nF, and model P-876K015, with a size of 50 mm × 11 mm and a capacitance of 16 nF. Both devices can be driven with a voltage excursion of ±100 V and show a very high input impedance (> 1 GΩ).

For testing the active optics technology we needed a compact electronics capable of driving up to 32 actuators, scalable to a higher number of channel if needed. Additionally, we chose to use a multichannel linear amplifier topology with static outputs rather than a multiplexed driver in order to eliminate any possible noise, during the optics testing, due to the switching of the multiplexer. A market survey showed that only general purpose and high cost electronic piezo drivers, designed for medium to large piezo actuators, were available and that they were not easily scalable.

So we decided to design and fabricate a dedicated electronic driving circuit. At this stage of the project, attention was focused more on circuit flexibility rather than ultimate optimization. As a consequence, circuit miniaturization and ultra low power consumption were traded off versus other parameters, such as scalability of the number of channels, circuit simplicity and stability, maximum output voltage and power supply efficiency.

3.2 Description of the driver electronics

We designed a compact electronic driver, able to drive up to 16 actuators, and built two identical electronics boxes to get a total of 32 channel for testing the optics. Several electronics boxes can be used together, so a large number of channel can be obtained if needed.

The driver system consists of the functional blocs shown in Figure 7: a control computer, a digital to analog converter (DAC), a multichannel high voltage linear amplifier, a power supply, and a high voltage DC-DC converter.

The signals controlling the multichannel piezo amplifier are generated by a commercial 16 channels Digital to Analog Converter (DAC), model USB-3105, manufactured by Measurement Computing Corporation. Each channel of the DAC can generate a voltage between -10 V and +10 V with a 16-bit resolution. The computer is actually a Raspberry Pi that acts as Ethernet instrument, accepting remote commands through a TCP/IP network while controlling the DAC through its USB connection. The low voltage output levels generated by the DAC are then amplified to the final output level by the high voltage amplifier. A 230 Vac to ±12 V power supply provides the dual voltage needed to power the electronics,

while the high voltage DC-DC converter, described in detail in Sect. 3.4, generates the ±100 V needed by the high voltage amplifier.

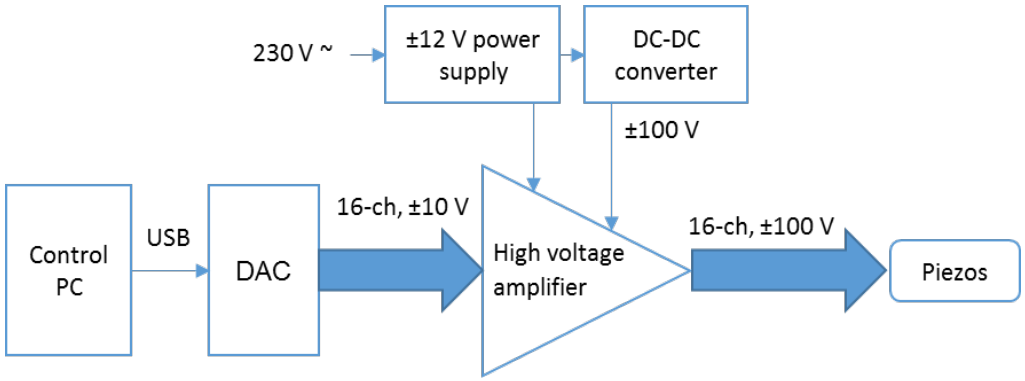

Figure 7. Driving electronics block diagram.

3.3 High voltage amplifier

As previously said, the voltage output of the DAC module covers the ±10 V range. However, to assess the active optics technology, we planned to test the piezo actuators within their full dynamic range, driving them with voltages between -100 V and +100 V. So a high voltage amplifier with a gain of 10 was needed.

At the beginning of the design process, a number of monolithic high voltage Operational Amplifiers (OP AMP) were considered for achieving such amplification, but they had to be ruled out due to their high power consumption and limited specifications. The typical quiescent current for a monolithic high voltage OP AMP is around 2.5 mA per channel which, considering for instance a maximum ±70 V dual supply, gives a power dissipation of 0.35 W per channel. Moreover, as we were already considering to increase the output voltage to ±100 V, no monolithic high voltage OP AMP's could comply with such specifications. As a consequence, a multichannel high voltage and low dissipation voltage amplifier had to be designed to the purpose.

The multichannel high-voltage amplifier is made by two 8-channels boards stacked together. The schematic diagram for a single channel is shown in Figure 8. The amplifier consists of two stages: the first stage is a conventional low voltage OP AMP, powered by the ±12 V dual supply and driving the high voltage output stage. In conventional amplifier design, the output stage is typically an emitter voltage follower obtained using a couple of complementary transistors. As a consequence, the driver stage needs to supply the full span of the desired output voltage. In order to avoid such a requirement and still employ a low voltage OP AMP, we chose a different approach for our design. The high voltage output stage consists of a pair of identical optocouplers, model TLP627 manufactured by Toshiba, whose output transistors are connected in series between the ±100 V dual supply voltages. It recalls a "totem pole" configuration, where the two optocouplers act as pull-up and pull-down devices. The LED's inside the optocouplers are driven in "push-pull" by the low voltage OP AMP. They are also slightly pre-biased, in order to reduce zero-crossing distortion. The optocouplers can thus be considered as a current amplifier, capable of managing high voltages. The voltage feedback, derived from the output voltage, guarantees the desired signal amplification and linearity.

There are many advantages in the proposed configuration. The OP AMP driving stage operates at low voltages. Furthermore, the output stage, based on optocouplers, has a quite small bias current (well below 0.1 mA). Both factors contribute to reach a very low quiescent power consumption which, in our circuit, is reduced to less than 15 mW per channel. Finally, the adopted optocouplers have a maximum operation voltage of 300 V. It means that the output stage is capable of managing output voltages between -150 V and +150 V. Further increase in the output voltage span can be achieved by simply using optocouplers with higher voltage capabilities.

The amplifier has a nominal overall voltage amplification of 10, with a bandwidth limited to 100 Hz because of the adopted dominant pole compensation for circuit stability. The bandwidth is, however, more than adequate to the typical control signals used to drive the piezo actuators. The total power consumption for the 16-channel voltage amplifier has been measured to be within 0.5 W and could be further reduced by selecting very low power OP AMP's.

The amplifier responses to a sinusoidal and a step stimulus coming from the DAC are shown, respectively, in Figure 9 and Figure 10.

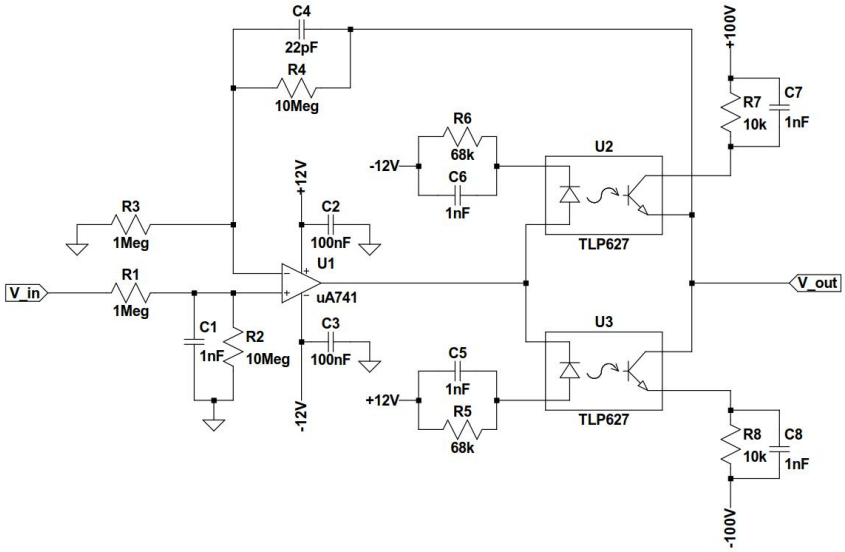

Figure 8. High-voltage amplifier schematic.

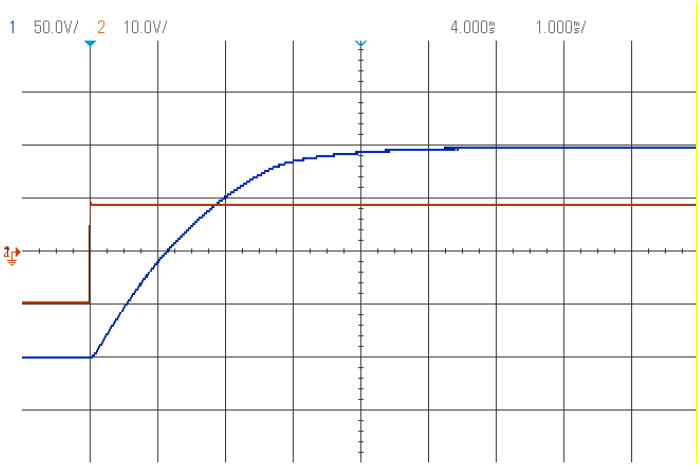

Figure 9. Measured response of the amplifier (blue, 50 V/div.) to a step stimulus (red, 10 V/div.). The output step covers the entire voltage range between -100 V and +100 V. Time scale is 1 ms/div.

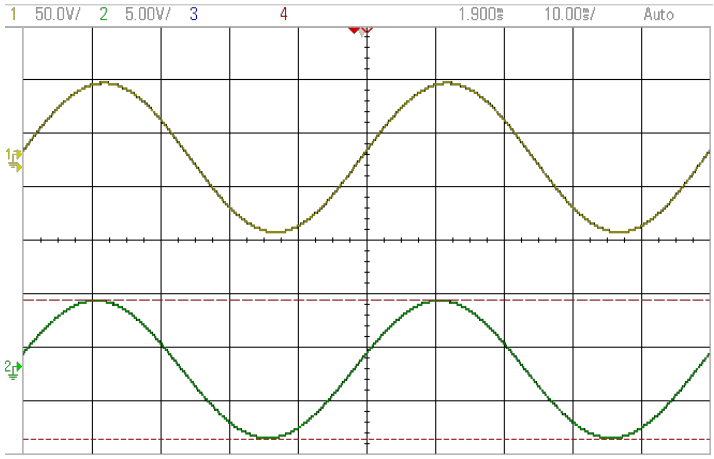

Figure 10: Signal response of the high voltage amplifier. A 20 Hz, 13V Pk-Pk sinusoidal input signal (below, 5 V/div.) is applied to the amplifier, producing a 140 V Pk-Pk output voltage (above, 50 V/div.). Time scale is 10 ms/div.

3.4 DC-DC converter

The high voltage DC-DC converter is based on a single-chip micropower isolated flyback converter, the LT8300 manufactured by Linear Technology. Using a double-secondary transformer with a 1:1:1 winding ratio, it produces a ±100 V dual voltage output, with a nominal maximum output power of 2 W, starting from a single 12 V input voltage. The circuit schematic is shown in Figure 11.

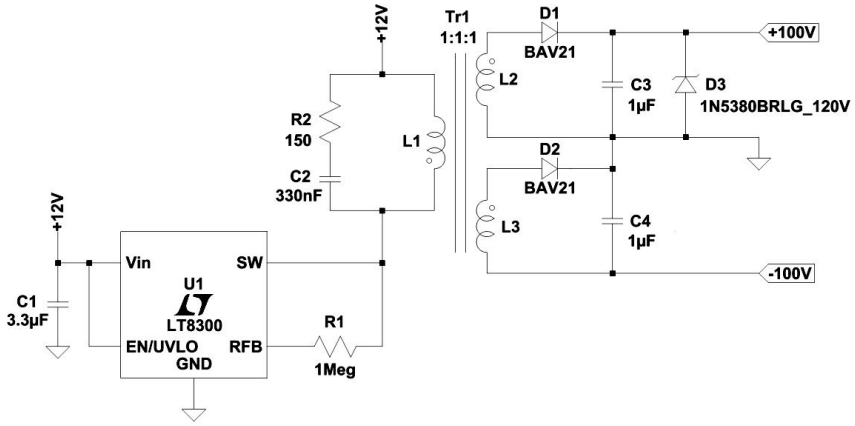

Figure 11. High voltage DC-DC converter schematic.

4 CONCLUSIONS

We have developed a simple, scalable and low-cost process to deposit electrical connections on the back of thin glass optics, to which piezoelectric actuators can be attached to build active X-ray optics. We also designed and built a driving electronics for the actuators in order to test the active optics prototypes. Details of the technological process and of the electronics design are shown here. Preliminary test results on the active optics can be found in [9].

5 ACKNOWLEDGMENTS

The AXYOM project, devoted to the study of the correction of thin glass/plastic foils for X-ray mirrors, is financed by a TECNO-INAF 2012 grant.

6 REFERENCES

[1] Civitani, M., Basso, S., Ghigo, M., Pareschi, G., Salmaso, B., Spiga, D., Tagliaferri, G., Vecchi, G., Burwitz, V., Hartner G. D., Menz, B., "X-ray optical units made of glass: achievements and perspectives," Proc. SPIE 9144, 914416 (2014), doi:10.1117/12.2056623

[2] Winter, A., Breunig, E., Friedrich, P., Proserpio, L., Döhring, T., "Indirect glass slumping for future x-ray missions: overview, status and progress," Proc. SPIE 9603, 96030S (2015), doi:10.1117/12.2188511

[3] Craig, W.W., An, H., Blaedel, K.L., et al., "Fabrication of the NuSTAR flight optics," Proc. SPIE 8147, 81470M (2011), doi: 10.1117/12.895278

[4] Civitani, M. M., Basso, S., Citterio, O., Conconi, P., Gallieni, D., Ghigo, M., Pareschi, G., Proserpio, L., Salmaso, B., Sironi, G., Spiga, D., Tagliaferri, G., Zambra, A., Martelli, F., Parodi, G., Fumi, P., Tintori, M., Gallieni, D., Bavdaz, M., Wille, E., "Accurate integration of segmented x-ray optics using interfacing ribs," Opt. Eng. 52(9), 091809-091809 (2013), doi:10.1117/1.OE.52.9.091809

[5] Salmaso, B., Basso, S., Civitani, M., Ghigo, M., Hołyszko, J., Spiga, D., Vecchi, G., Pareschi, G., "Slumped glass optics development with pressure assistance," Proc. SPIE 9905, 990523 (2016), doi:10.1117/12.2187539

[6] Spiga, D., Barbera, M., Collura, A., Basso, S., Candia, R., Civitani, M., Di Bella, M., Di Cicca, G., Lo Cicero, U., Lullo, G., Pelliciari, C., Riva, M., Salmaso, B., Sciortino, L., Varisco, S., "Manufacturing an active X-ray mirror prototype in thin glass," Journal of Synchrotron Radiation 23(1), 59 (2016), doi:10.1107/S1600577515017142

[7] Spiga, D., Barbera, M., Basso, S., Civitani, M., Collura, A., Dell'Agostino, S., Lo Cicero, U., Lullo, G., Pelliciari, C., Riva, M., Salmaso, B., Sciortino, L., "Active shape correction of a thin glass/plastic x-ray mirror," Proc. SPIE 9208, 92080A (2014), doi:10.1117/12.2063349

[8] Spiga, D., Barbera, M., Collura, A., Basso, S., Candia, R., Civitani, M., Di Bella, M., Di Cicca, G., Lo Cicero, U., Lullo, G., Pelliciari, C., Riva, M., Salmaso, B., Sciortino, L., Varisco, S., "Manufacturing and testing a thin glass mirror shell with piezoelectric active control," Proc. SPIE 9603, 96031N (2015), doi:10.1117/12.2189990

[9] Spiga, D., Barbera, M., Collura, A., Basso, S., Candia, R., Civitani, M. M., Di Cicca, G., Lo Cicero, U., Lullo, G., Pelliciari, C., Salmaso, B., Sciortino, L., Varisco, S., "Realization and drive tests of an active thin glass x-ray mirror," Proc. SPIE 9965, this conference (2016).